Magnetic and Thermal Properties of Semimagnetic Semiconductors

L. A. Wahab[1,*], N. M. Yousif[1], L. Kilanski[2] and K. Swiatek[2]

[1]Thermal and Magnetic Laboratory, National Center for Radiation Research and Technology, Egyptian Atomic Energy Authority, Cairo, Egypt
[2]Institute of Physics, Polish Academy of Sciences, Warsaw, Poland
[*]Corresponding author: aly_lo2003@yahoo.com

Measurements of the dynamic magnetic susceptibility χ as a function of temperature were made on polycrystalline semimagnetic semiconductor $Cd_{1-x}Mn_xSe$ (x = 0.1, 0.2 and 0.3). The magnetic susceptibility was investigated in the temperature range of 5-200K revealing the paramagnetic behavior described by the Curie-Weiss law and indicating the presence of antiferromagnetic exchange interactions between Mn ions. The $1/\chi_m$ versus T curves indicates that for x=0.1 the behavior was a mixture of antiferromagnetic and spin-glass while for x = 0.2 and 0.3 shows spin-glass form. The temperature dependence of the EPR spectra for the investigated samples was measured in the temperature range 4 to 300k. The obtained g-factor of the investigated samples shows slight decrease with increasing the concentration of Mn. The calculated number of defects illustrates that increasing the temperature leads to an increase in the number of defects increases.

1. Introduction

Diluted magnetic semiconductors (DMS) are semiconductor materials in which a fraction of sublattice is replaced by other metal ion having a magnetic moment **[1]**. These materials exhibit a wide range of magnetic properties including paramagnetic, spin glass, or ferri/ferro-magnetic behavior. DMS have received attention due to their potential usage in magnetic applications including spintronics, magnetic switching, magnetic recording, and the so-called future High-Tech electronics **[2]**.

Semiconductor materials containing manganese are of interest because of the manner in which the magnetic behavior is associated with the manganese can modify and complement the semiconductor properties **[3, 4]**. Hence, the behavior of the compounds is either paramagnetic, spin glass or antiferromagnetic, depending on concentration of Mn **[5]**.

The study of some magnetic properties of the compounds represents a convenient method of determining the degree of order in such alloys. It has been

shown for $MnIII_2VI_4$ compounds, that, those alloys in which the Mn is disordered, have very different magnetic behavior from those showing an ordered Mn arrangement **[6-7]**. The study found that when the Mn atoms are ordered on the cation sublattice the compound shows almost ideal antiferromagnetc behavior. However, when the Mn atoms are randomly mixed on the sublattice the compound spin-glass behavior is shown. It was found that the values of the Curie-Weiss constant θ, determined from magnetic susceptibility measurements, gave a good indication of the ordered arrangement of the Mn atoms in various materials.

EPR spectroscopy is used in various branches of science such as chemistry and physics, for the detection and identification of free radicals and paramagnetic centers.

The aim of the present study is to prepare the ternary compounds $Cd_{1-x}Mn_xSe$ (x= 0.1, 0.2, 0.3) and to study structure, magnetic and thermal properties.

2. Experimental

$Cd_{1-x}Mn_xSe$ semimagentic semiconductor materials with different concentrations of Mn for x= 0.1, 0.2, and 0.3 were prepared by the melt quenching technique. Appropriate amounts of Cd, Mn and Se elements of 5N nominal purity were sealed in evacuated quartz ampoules (10^{-5} Torr). The evacuated ampoules were then placed in a furnace whose temperature was raised gradually and kept constant for 2h at 500^{o}C and then at 1000^{o}C for 25h. The melt was then quenched in ice water. The long duration of alloying and the continuous shaking of the melt in the furnace ensure the homogeneity of the compositions of the samples under test. The chemical composition of the samples was obtained through the energy dispersive X-ray (EDX) analysis. The structure was determined by powder X-ray diffraction XRD using a Shimadzu X-ray machine, in the 2θ range 4-90^o, with CuK_α tube (λ=1.54Å) at room temperature to obtain crystal phase and structural information of the samples. The transition temperatures were determined using the Shimadzu instrument, differential thermal analysis (DTA-50). The measurements were carried out under nitrogen atmosphere (20 cm^3 min^{-1}). Rietveld refinement profile of the powder XRD patterns of $Cd_{1-x}Mn_xSe$ (x= 0.1, 0.2, 0.3) used a pcw program to calculate both grain size and lattice parameters. The Ac magnetic susceptibility measurements were carried out in the temperature range 4-200K using mutual inductance method employed into the LakeShore 7229 susceptometer with applied field of H=10 Oe and applied frequency f = 625Hz. The EPR spectra were obtained from powdered samples, using a standard Bruker ESP 300E equipment operating in varian E-line X-band spectrometer with microwave frequency (f ≈ 9-10 GHz), modulation field (H_m ≈ 0.1G), microwave puissance (P_H = 2 mW) and gain detection (G_e = 10000). A continuous flow helium cryostat (Oxford Instrument ESR-9) was used to control temperatures in the interval 4-300 K with an accuracy of ± 1K.

3. Results and Discussion

Elemental analysis techniques are used simply to give an image about the elements ratio in the samples. The data obtained from EDX indicate that all samples show the exact match for standard peak position for Cd, Se and M, Table (1).

Table (1): illustrated the atomic % of $Cd_{1-x}Mn_xSe$ samples.

Composition	Cd %	Mn %	Se%
$Cd_{0.9}Mn_{0.1}Se$	46.262	5.000	48.740
$Cd_{0.8}Mn_{0.2}Se$	43.110	14.725	42.165
$Cd_{0.7}Mn_{0.3}Se$	36.053	20.827	43.120

X-ray difractograms for $Cd_{1-x}Mn_xSe$ (x= 0.1, 0.2, 0.3) were depicted in Fig. (1). All the prepared samples are single phase. The X-ray patterns were identified using the JCPDS card No. 65-3415 for the hexagonal system. In the present study, Rietveld quantitative phase analysis was applied to identify the position of Cd, Mn and Se. Fig. (2) shows the refinement profile of $Cd_{0.7}Mn_{0.3}Se$ as an example. It should be noted that there are no traces or additional phases corresponding to Mn or any binary phase. The crystallite size were obtained from the full width at half-maximum (FWHM) of the diffraction peaks. Table (2) illustrates that the calculated crystal size decreased by the increasing of Mn content. This behavior is interpreted depending on both the ionic size and oxidation state of dopants where the ionic size of Mn^{+2} = 0.81 Å while that of Cd^{+2} = 1.09 Å [8].

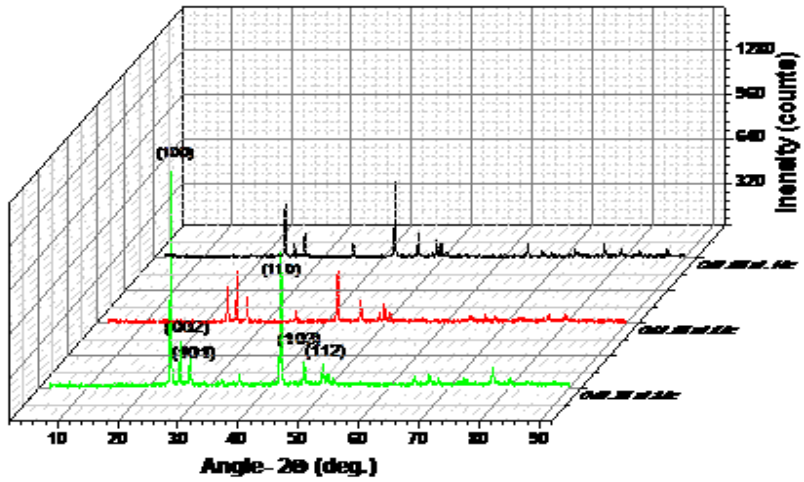

Figure (1): X-ray diffraction patterns of the investigated samples.

The kinetics of the crystallization process of the investigated samples were studied through determination of the kinetic parameter n (which reflects the nucleation rate and/or the growth morphology) and the activation energy E of the process. Non-isothermal single scan technique was applied to study thermally

activated phenomena in the investigated compounds. This was carried out using a constant slow scan rate ($\varphi = dT/dt = 5\,^{\circ}\mathrm{C min}^{-1}$) was used. The thermograms are characterized by the presence of an endothermic peak due to softening (T_g), and exothermic peak due to crystallization (T_c). The transition temperatures T_g and (T_c) are listed in Table (3).

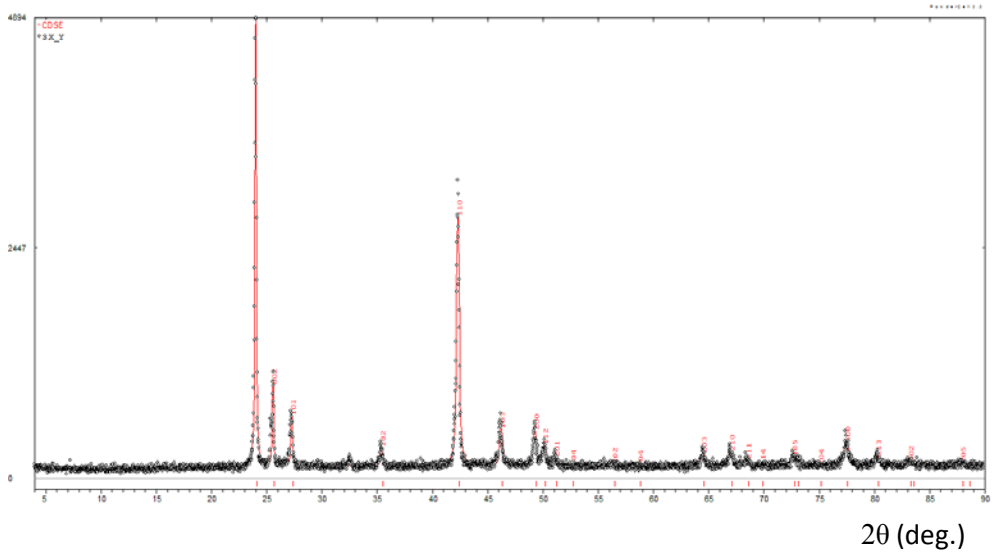

Figure (2): The profile fitting of $Cd_{1-x}Mn_xSe$.

The formal theory of transformation kinetics can be used to describe the kinetics of non-isothermal crystallization [9–11]:-

$$\boldsymbol{\alpha = 1 - \exp\left(-Kt^{n}\right)} \tag{2}$$

$\boldsymbol{\alpha}$ is the crystallized fraction in time t, and $\boldsymbol{K}$ the reaction rate constant usually assigned an Arrhenian temperature dependence

$$\boldsymbol{K = K_0 \exp(-E/RT)} \tag{3}$$

K_0 is the frequency factor. The two former equations are often used to deduce relationships describing non-isothermal crystallization processes. We then have

$$\boldsymbol{\ln\{-\ln(1-\alpha)\} = \ln K_0 - ER/T + n \ln t} \tag{4}$$

at constant t, a plot of $\ln\{-\ln(1-\alpha)\}$ against $1/T$ can be used to obtain E. A recent study **[12]** has shown that a simple DTA model using a single scan technique can be used to study thermally activated crystallization in amorphous semiconductors. In this model, the assumption is made that the extent of α is proportional to the relevant area under the DTA peak. Accordingly, a plot of log $[g(\alpha)]$ versus $1/T$ yields a straight line when an appropriate mathematical description of the reaction is given by

$$\boldsymbol{\log[g(\alpha)] = \ln\left[K_o^{1/n}/\varphi R\right] - E/nRT} \tag{5}$$

Table (2): Grain size, Lattice parameters and Magnetic parameters of the $Cd_{1-x}Mn_xSe$ samples.

Composition	Grain Size (nm)	Lattice parameters (Å)		θ_p (K)	C_M (emu/mole)	χ_0	J	μ_{eff} (exp.) (μ_B)
		a	**c**					
$Cd_{0.9}Mn_{0.1}Se$	115.84	4.28	6.98	-40	0.88318	-0.0042	45.3	8.5
$Cd_{0.8}Mn_{0.2}Se$	61.75	4.26	6.95	-157	2.42831	-0.00432	64.7	10
$Cd_{0.7}Mn_{0.3}Se$	58.00	4.25	6.93	-167	3.77845	-0.0095	44.2	10.2

$\boldsymbol{K_0}$ is considered to be constant with respect to temperature and φ *the heating rate*. The slope of $\log[g(\alpha)]$ versus $1/T$ gives the value of E/n. Calculation of the function $g(\alpha)$ has been carried out by Skavara and Stava for different reaction kinetic equations and nine kinetic equations for different reaction processes with their function symbols reported **[14,15]**. From the function $g(\alpha)$ of all the reaction kinetic equations it is found that the best fit for the increasing part of the two crystallization peaks is obtained for the function $A_3\{A_3 = [-\ln(1-\alpha)]^{1/3} = KT\}$. $A3$ indicates the presence of random nuclei in the as- quenched $Cd_{1-x}Mn_xSe$ materials and that the growth of these nuclei is being diffusion -controlled. Fig. (3) shows the plot of log $[g(\alpha)]$ versus $1/T$ for the studied compound using the appropriate choice of A_3. From the slopes of the straight portions ,the values of the effective activation energies E/n can be estimated. The values of n is calculated from the slope of $\ln[-\ln(1-\alpha)]$ versus $1/T$ given in Fig. (4). Table (4) gives the values of E and n for the investigated samples. The values of n indicate that the growth of the random nuclei, formed in the as quenched ingots, takes place in three dimensions. It is clear from the table that the crystallization energy increases with increasing Mn which means that the addition on Mn impedes the crystallization process.

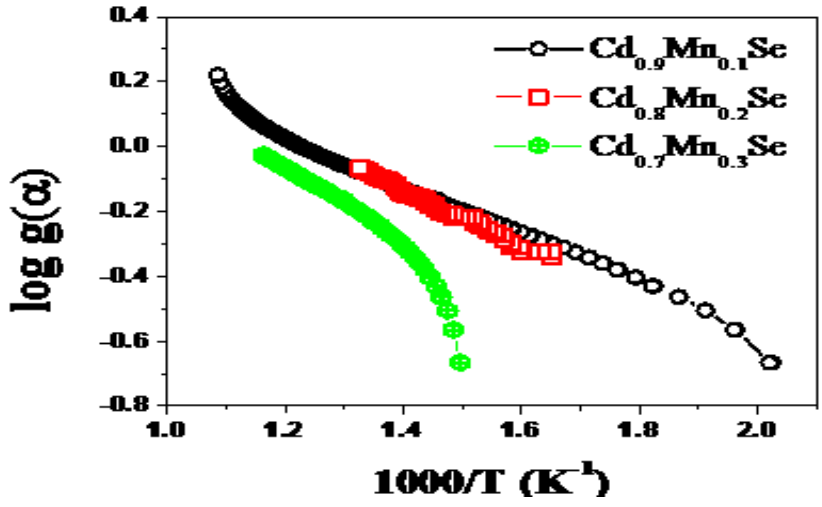

Figure (3): A plot of ln g(α) vs. 1000/T of $Cd_{1-x}Mn_xSe$ samples.

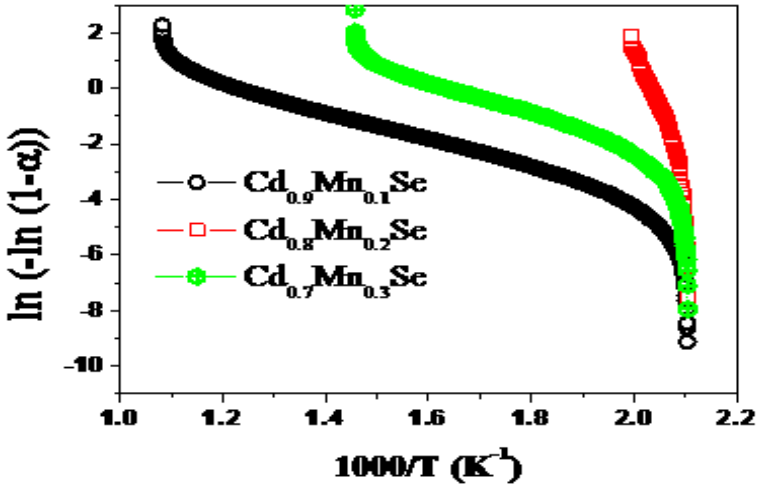

Figure (4): A plot of ln(-ln(1-α)) vs. 1000/T of $Cd_{1-x}Mn_xSe$ samples.

Table (3): Thermal transition temperatures of the investigated samples.

Compositions	**T_g ˚C**	**T_c ˚C**	
		T_c^{Begin}	**T_c^{peak}**
$Cd_{0.9}Mn_{0.1}Se$	286.65	300.72	556.63
$Cd_{0.8}Mn_{0.2}Se$	270	319.26	626.29
$Cd_{0.7}Mn_{0.3}Se$	257.90	383.52	666.44

The temperature dependence of the magnetic susceptibility of the investigated samples is given in Fig. (5). The figure illustrates that the prepared samples are paramagnetic materials. At law Mn concentrations, most Mn ions have no Mn neighbors in the nearest shells, and the Mn subsystem demonstrates paramagnetic properties. It is clear that the paramagnetic susceptibility of the investigated samples increases with increasing the Mn content.

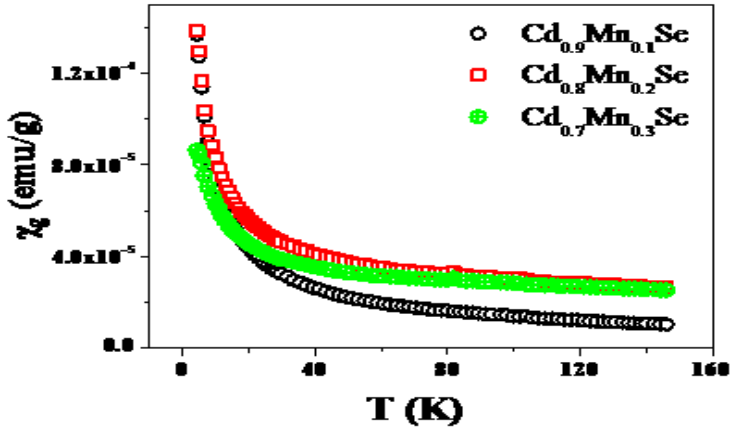

Figure (5): Magnetic susceptibility temperature dependence of $Cd_{1-x}Mn_xSe$ samples.

Figure (6) shows the temperature dependence of the inverse of the magnetic susceptibility for the investigated samples. These data collapse to straight lines, indicating a Curie-Weiss-type magnetic behavior following the

$$X_M = X_o + C_M/(T- \theta_p) \quad (6)$$

and

$$C_M = \mu^2_{eff} N_A x/3K_B$$

where X_o is the molar susceptibility of the host matrix, C_M is the molar Curie constant, θ_p the paramagnetic Curie temperature, T absolute temperature, N_A is Avogadro's number, x is the mole fraction of Mn in the glass, K_B the Boltzmann's, and μ_{eff} is the effective magnetic moment.

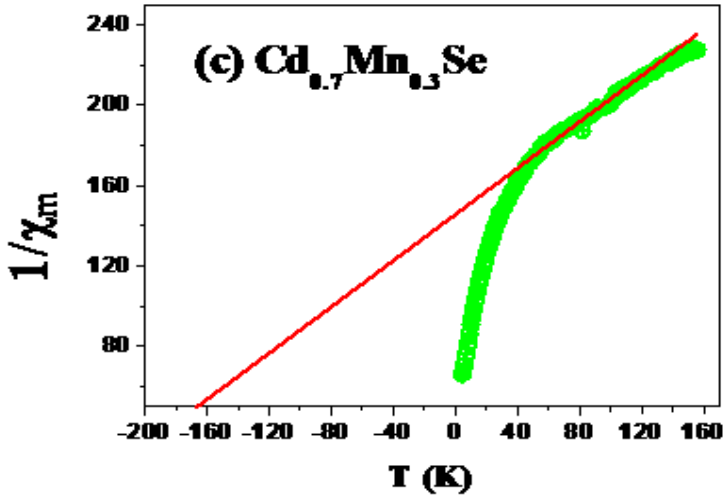

Figure (6): The inverse of molar susceptibility dependence of temperature of the $Cd_{0.7}Mn_{0.3}Se$ sample.

Table (4): The crystallization activation energy, crystallization order n, and the crystallity fraction α for the investigated compositions.

Composition	E (kcal/mole)	Crystallization order , n	Range α
$Cd_{0.9}Mn_{0.1}Se$	10.7146	2.9	0.12 : 0.99
$Cd_{0.8}Mn_{0.2}Se$	11.415	2.8	0.19 : 0.99
$Cd_{0.7}Mn_{0.3}Se$	20.25	2.6	0.147 : 0.922

Figure (6) illustrates that in the case of $Cd_{0.7}Mn_{0.3}Se$ sample, the $1/\chi$ versus temperature graph is linear at higher temperatures, but shows a deviation from the Curie-Weiss form for temperatures below 40 K. This indicates typical spin-glass form. Value of θ_p is obtained from the higher temperature range of this curve. The deviations from Curie-Weiss behavior indicate that Mn atoms are randomly distributed with antiferromagnetic interaction between the Mn atoms. This means

that the disorder increased with increasing the amount of Mn. The paramagnetic Curie-Weiss temperature, θ_p, is a rough indicator of magnetic interaction between the Mn ions, and its sign depends on whether the interaction helps align adjacent moments in the same direction or opposite to one another. The obtained values of θ_p are given in Table (2), the negative values suggest that the interaction between the Mn ions helps to align adjacent moments opposite to each other, and there is a net antiferromagnetic interaction between moments. The obtained data shows that θ_p increases with the increase of Mn ions content; this implies stronger interactions and more ions participating in the interactions.

When a magnetic field is applied to a magnetic material, its magnetic moments tend to align themselves in the magnetic field direction and a more ordered state is achieved, so the magnetic entropy of the system decreases. In an isothermal process of magnetization, the magnetic entropy change of the system due to the application of the magnetic field, ΔS_M, can be derived from Maxwell relations **[16].**

$$\mathbf{\Delta S_M\ (T,\ H) = \int_{H_{min}}^{H_{max}} \left(\frac{\partial M}{\partial T}\right)_H dH} \qquad (7)$$

where
H_{min} and H_{max} represent the initial and finial values of the magnetic field. It is clear that high magneto- caloric effect will be observed when the temperature dependence of the magnetization (i.e.) is high. This occurs, for example, at the Curie temperature of ferromagnetic- paramagnetic transition (at which the maximum absolute value of the entropy change is expected) and at low temperatures for paramagnetic materials. Measurements of magnetic entropy variation when fixed magnetic fields change is applied makes it possible to determine whether a magnetic material may be considered to be a good magnetic refrigerant. Thus, for Curie-Weiss paramagnets the entropy change ΔS_M will be [17]:-

$$\mathbf{\Delta S_M = -\frac{C_M}{2}\frac{\Delta H^2}{(T-\theta_p)^2}} \qquad (8)$$

The temperature dependence of the entropy obtained for different concentrations of Mn in compound of the investigated samples is shown in Fug. (7).

It is clear that the entropy decreases with the increase of temperature. This behavior is expected for paramagnetic materials because their magnetization increases quickly when the temperature decreases. Because of their paramagnetic behavior at low temperatures, the investigated materials exhibit the entropy change that rapidly increases when the temperature decreases. This means that the materials can be used as active magnetic refrigerants at low temperatures.

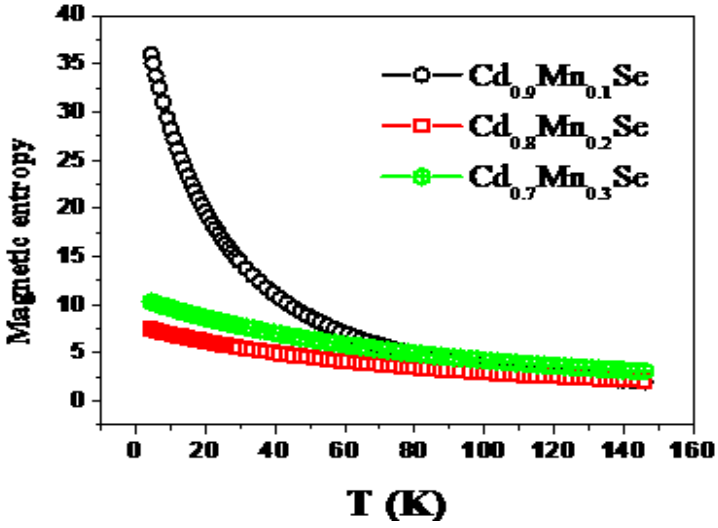

Figure (7): Temperature dependence of the magnetic entropy of the investigated samples.

Figure (8) shows the representative EPR spectra of the investigated samples at various temperatures. The figure illustrates that the spectra are narrow and symmetric with Lorentzian shape, typical for paramagnetic. The area under curve, which is proportional to the sample magnetization, decreased systematically as the temperature increased. The peak to peak line width (ΔH) has tendency to decrease with increasing temperature up to 300 K (Figure (9).

The g-value has been determined using the following equation:

$$g_e = h\,\upsilon / \mu_B B_0 \qquad (9)$$

where

h is Plank's constant = $6.6260693 \times 10^{-34}$ J.s, μ_B is Bohr magneton= $9.27400949 \times 10^{-24}$ J.T^{-1}, 1 T= 10000 G, and υ is microwave frequency= 9.45 GHz. The obtained g- factor of the investigated samples is 2.006, 2.003, and 1.997 for $Cd_{0.9}Mn_{0.1}Se$, $Cd_{0.8}Mn_{0.2}Se$, and $Cd_{0.7}Mn_{0.3}Se$, respectively. This shows that the value of g- factor slightly decreases with increasing the concentration of Mn of compound. The g-factor varies depending on the electronic configuration of the radical or ion also represent spectroscopic splitting. An unpaired electron can gain or lose angular momentum, which can change the value of g-factor, causing it to differ from g_e. This is especially significant for chemical systems with transition-metal ions.

The number of defects in the investigated compounds were obtained from the following formula:-

$$N = K \frac{H_0 (\Delta H)^2 (A/2)}{G_e \sqrt{P_H}\, H_m} \qquad (10)$$

where

N is the number of defects, K is constant of spectrum $\approx 9.1 \times 10^{12}$, H_0 is the magnetic field corresponding to the center of signal, Δ **H** is the width of the magnetic field from peak to peak (G), **A** is the height of the signal (cm), $\mathbf{H_m}$ is modulation field (0.1 G Gs), $\mathbf{P_H}$ is microwave Puissance (2 mW), and $\mathbf{G_e}$ is gain detection (10000). Table (5) illustrates the number of defects at different temperatures of the investigated samples. It is clear from the table that as the temperature increases, number of defects or number of free radical increases.

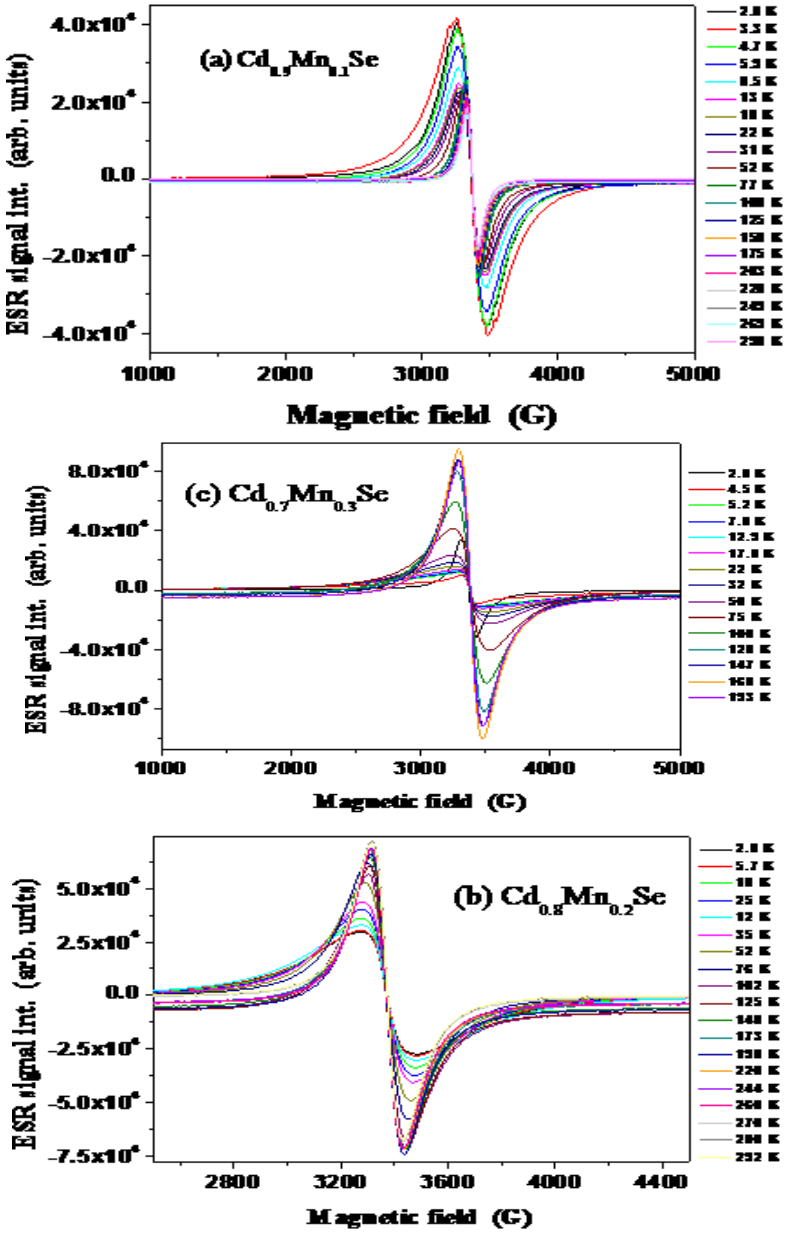

Figure (8): EPR spectra for the investigated samples (a) $Cd_{0.9}Mn_{0.1}Se$, (b) $Cd_{0.8}Mn_{0.2}Se$, and (c) $Cd_{0.7}Mn_{0.3}Se$.

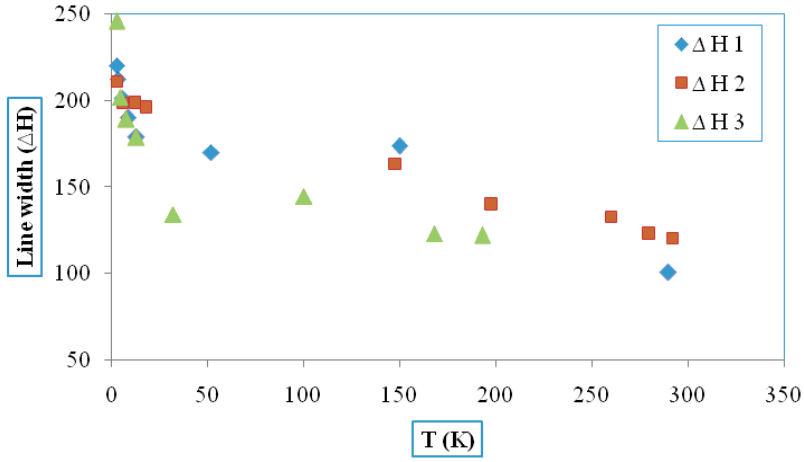

Figure (9): The line width as a function of temperature for the investigated samples.

4. Conclusion

Nanocrystalline bulk samples $Cd_{1-x}Mn_xSe$ (x = 0.1, 0.2 and 0.3) were prepared by melt quenching in ice-water. Thermal analysis studies showed that the activation energy of crystallization increases with increasing Mn content, which means that Mn impedes the crystallization process. Temperature dependence of the magnetic susceptibility of the investigated samples shows that the prepared samples are paramagnetic materials. The molar Curie constant, the molar susceptibility of the host matrix, the effective magnetic moment and paramagnetic Curie temperature increased with the increasing of Mn ions content. This implies stronger interactions and more ions participating in the interactions. The deviations from Curie-Weiss behavior indicate that Mn atoms are randomly distributed with strong antiferromagnetic interaction between the Mn atoms. The number of defects are shown to increase with increasing temperature.

References

1. Tianhao Ji, Wen-Bin Jian, Jiye Fang, Jinke Tang, Volodymyr Golub, and Leonard Spinu, *IEEE Transcations on Magnetics*, **39**, 2791 (2003).
2. V.S. Karande, S.H. Mane, V.B. Pujari, L.P. Deshmukh, *J. Matterials Letters*, **59**, 148 (2005).
3. M. Quintero, M. Morocoima, A. Rivero, P. Bocaranda and J.C. Woolley, *J. Phys. Chem. SAolids*, **58**, 491 (1997).
4. A.I. Savchuk, I.D. Stolyarchuk, S.V. Medynskiy, V.I. Fediv, Ye.O. Kandyba, A. Perrone, M.L. DeGiorgi, P.I. Nikitin, *J. Materials Science and Engineering* C, **15**, 79 (2001).
5. K.P. Reddy, N. Madusudhana, D.R. Reddy, B.K. Keddy, *J. Spectrochimica Acta Part*, **A61**, 3056 (2005).

6. J.C. Wolley, S. B ass, A.M. Lamarche, G. Lamarche, *J. Mag. Mag. Mat*., **131**, 199 (1994).
7. L.A. Wahab, N. Makram, H.H. Hantour, *Journal of Radiation Research & Applied Science*, **7**, 55 (2014).
8. Pauling, L. "The Nature of the Chemical Bond" (3rd Edn.), Ithaca, NY: Cornell University Press, (1960).
9. M.Avrami, *J. chem. Phys*., **7**, 1103 (1939).
10. M.Avrami, *J. chem. Phys*., **8**, 212 (1940).
11. M.Avrami, *J. chem. Phys*., **9**, 117 (1941).
12. L.A. Wahab, *Indian Journal of Pure & Applied Physics*, **40**, 873 (2002).
13. L.A. Wahab, M.B. El-Den, A. Adam, M.H. Anoar and R.A. Khadoor, A-*Azhar Bull. Sci*., Vol. **18**, 81 (2007).
14. J.Sestak, *J. Phys. and Chem. Glasses*, **15**, 6, 137 (1974).
15. V.Stava, *Thermochim Acta*, **2**, 423 (1971).
16. Antonio Fernandez, Xavier Bohigas, Javier Tejada, Elena A. Sulyanova, Irina I. Buchinskaya, and Boris P. Sobolev; *Mater. Chem. Phys*., **105**, 62 (2007).
17. A.M. Tishin, Y.I. Spichkin; *The Magnetocaloric Effect and its Applications, Institute of Physics Publishing*, **1** (2003).